Small-Angle Neutron Scattering and Surface Force Investigations of Poly(amido amine) Dendrimer with Hydroxyl End Groups†

Toyoko Imae,*,‡ Katsuya Funayama,‡ Keigo Aoi,§ Kaname Tsutsumiuchi,§ Masahiko Okada,§ and Michihiro Furusaka||

Graduate School of Science and School of Agricultural Sciences, Nagoya University, Chikusa, Nagoya 464-8602, Japan, and Institute of Materials Structure Science, High Energy Accelerator Research Organization (KEK), Tsukuba 305-0801, Japan

Received September 8, 1998. In Final Form: February 8, 1999

Atomic force microscopic image on mica substrate, which was dipped for 10 min in an aqueous solution of fifth-generation poly(amido amine) dendrimer with hydroxyl end groups, displayed a flatter texture of dendrimer-adsorbed surface. On the external contrast variation of small-angle neutron scattering for aqueous dendrimer solutions, the apparent radius of gyration of dendrimer decreased with increasing H_2O content in H_2O/D_2O mixed solvent, indicating the water penetration into dendrimer. The calculation based on small-angle neutron scattering theory and a five-layer model of dendrimer with water penetration was fitted with the observed one. In connection with the ability of dendrimer doping small molecules, it is confirmed that the segment density profile in dendrimer is owing to the compensation of the segment density increase by the segment branching and the density decrease due to the segment chain extension, although the water penetration depends on the latter fact. The surface force−separation curves between glass beads adsorbed dendrimers in aqueous solutions depended on the adsorption time. At a medium adsorption time, the electrostatic repulsion force between glass surfaces diminished apparently owing to the adsorption of dendrimers. Moreover, dendrimers sandwiched between glass surfaces raised the adhesive attraction force with glass surfaces. At a long adsorption time, both glass surfaces were covered by adsorbed dendrimers, and the repulsive force acted between dendrimer layers. Same profiles of the surface force−separation curves were observed at a shorter adsorption time for the more concentrated solution and for the higher-generation dendrimer. It is confirmed from the theoretical analysis that the interaction force between dendrimer layers is dominated by the osmotic pressure effect in the steric repulsion force. This suggests the utilization of poly(amido amine) dendrimer with a hydroxyl end groups as a surface-improvement agent promoting the dispersion stability of fine particles in medium.

Introduction

Dendritic macromolecules, that is, dendrimers, have well-defined three-dimensional structure which is built up by the successive synthesis of branching portions from a multifunctional central core.[1−3] The size and shape of dendrimers are comparable to those of micelles, microemulsions, and vesicles, which are self-assembled in solutions. Therefore, for dendrimers, one can expect the functions as well as the self-assembled particles and, moreover, the additional novel functions owing to the less compact structure of the dendrimer.

Hitherto, novel dendrimers such as polystyrene−dendrimer amphiphilic copolymers,[4,5] amphiphilic star copolymers with dendritic moieties,[6] mesogen-substituted carbosilane dendrimers,[7] mono- and polydendron,[8−10] nitroxyl-functionalized dendrimers,[11] dendrimers possessing internal electroactive anthraquinoid,[12] and dendrimers with paramagnetic and diamagnetic cores[13] have been synthesized, and their aggregation morphology, stimuli-response, film morphology, characterization, exchange interaction, electrochemical reaction, and molecular dynamics have been investigated.

One of the more investigated dendrimers is poly(amido amine) (PAMAM) dendrimer and its derivatives.[1,14−24]

* To whom correspondence should be addressed.

† Presented at Polyelectrolytes '98, Inuyama, Japan, May 31−June 3, 1998.

‡ Graduate School of Science, Nagoya University.

§ School of Agricultural Sciences, Nagoya University.

|| Institute of Materials Structure Science.

(1) Tomalia, D. A.; Naylor, A. M.; Coddard, W. A., III *Angew. Chem., Int. Ed. Engl.* **1990**, *29*, 138.
(2) Frechet, J. M. J. *Science* **1994**, *263*, 1710.
(3) Newkome, G. R.; Moorefield, C. N.; Vogtle, F. In *Dendritic Molecules: Concepts, Synthesis, Perspectives;* VCH: Weinheim, 1996.
(4) van Hest, J. C. M.; Delnoye, D. A. P.; Baars, M. W. P. L.; van Genderen, M. H. P.; Meijer, E. W. *Science* **1995**, *268*, 1592.
(5) van Hest, J. C. M.; Baars, M. W. P. L.; Elissen-Román, C.; van Genderen, M. H. P.; Meijer, E. W. *Macromolecules* **1995**, *28*, 6689.
(6) Gitsov, I.; Fréchet, J. M. J. *J. Am. Chem. Soc.* **1996**, *118*, 3785.
(7) Coen, M. C.; Lorenz, K.; Kressler, J.; Frey, H.; Mülhaupt, R. *Macromolecules* **1996**, *29*, 8069.
(8) Kaneko, T.; Horie, T.; Asano, M.; Aoki, T.; Oikawa, E. *Macromolecules* **1997**, *30*, 3118.
(9) Hudson, S. D.; Jung, H.-T.; Percec, V.; Cho, W.-D.; Johansson, G.; Ungar, G.; Balagurusamy, V. S. K. *Science* **1997**, *278*, 449.
(10) Percec, V.; Ahn, C.-H.; Ungar, G.; Yeardley, D. J. P.; Moller, M.; Sheiko, S. S. *Nature* **1998**, *391*, 161.
(11) Bosman, A. W.; Janssen, R. A. J.; Meijer, E. W. *Macromolecules* **1997**, *30*, 3606.
(12) Newkome, G. R.; Narayanan, V. V.; Echegoyen, L.; Pérez-cordero, E.; Luftmann, H. *Macromolecules* **1997**, *30*, 5187.
(13) Gorman, C. B.; Hager, M. W.; Parkhurst, B. L.; Smith, J. C. *Macromolecules* **1998**, *31*, 815.
(14) Bauer, B. J.; Briber, R. M.; Hammouda, B.; Tomalia, D. A. *Polym. Mater. Sci. Eng.* **1992**, *66*, 428.
(15) Briber, R. M.; Bauer, B. J.; Hammouda, B.; Tomalia, D. A. *Polym. Mater. Sci. Eng.* **1992**, *67*, 430.
(16) Meltzer, A. D.; Tirrell, D. A.; Jones, A. A.; Inglefield, P. T.; Hedstrand, D. M.; Tomalia, D. A. *Macromolecules* **1992**, *25*, 4541.
(17) Haensler, J.; Szoka, F. C., Jr. *Bioconjugate Chem.* **1993**, *4*, 372.
(18) Aoi, K.; Itoh, K.; Okada, M. *Macromolecules* **1995**, *28*, 5391.
(19) Wells, M.; Crooks, R. M. *J. Am. Chem. Soc.* **1996**, *118*, 3988.
(20) Cooper, A. I.; Londono, J. D.; Wignall, G.; McClain, J. B.; Samulski, E. T.; Lin, J. S.; Dobrynin, A.; Rubinstein, M.; Burke, A. L. C.; Fréchets, J. M. J.; DeSimone, J. M. *Nature* **1997**, *389*, 368.
(21) Pistolis, G.; Malliaris, A.; Paleos, C. M.; Tsiourvas, D. *Langmuir* **1997**, *13*, 5870.

10.1021/la9811968 CCC: $18.00
Published on Web 04/06/1999

PAMAM dendrimer has first been synthesized by Tomalia et al.,[1] and its solution behavior has been studied by small-angle neutron scattering (SANS).[14,15] The gene carrier ability of PAMAM dendrimer has been investigated by Haensler and Szoka.[17] Meltzer et al.[16] have synthesized the PAMAM dendrimer with hydroxyl end groups and studied ^{13}C NMR relaxation parameters. The binding of fluorescent probe molecules to PAMAM dendrimers has been investigated by Pistolis et al.[21] Wells and Crooks[19] have constructed a chemically sensitive dendrimer layer by linking PAMAM dendrimers to a mercaptoundecanoic acid self-assembled monolayer via amide bond formation. The interactions between PAMAM dendrimer surfaces and vapor phase probe molecules have been elucidated. The investigation of chemically sensitive surfaces has also been performed for a poly(iminopropane-1,3-diyl) dendrimer.[25] The functionalization of PAMAM dendrimer is attained by the modification of its exterior.[18,20,22−24] Aoi et al.[18,23,24] have synthesized sugar-persubstituted PAMAM dendrimer, linear polymer/PAMAM dendrimer amphiphilic block copolymer, and amphiphilic hemispherical block dendrimer. Cooper et al.[20] have synthesized dendritic surfactants with fluorinated shell and reported the effective extraction of a hydrophilic compound from water into liquid CO_2. Thornton et al.[22] have investigated the chromophore-functionalized PAMAM dendrimers.

In the present work, the adsorption of PAMAM dendrimers with hydroxyl end groups on mica substrate is characterized by atomic force microscopy (AFM). The solution properties are examined by SANS, and the solid−liquid interface adsorption behavior is investigated by surface force apparatus. The adsorption of dendrimers on glass surface and the interaction forces between dendrimer-adsorbed layers have never been reported yet. A SANS investigation of aqueous PAMAM dendrimer solutions has been reported by Bauer et al.[14] and Briber et al.[15] They investigate the particle properties and the intermolecular interactions depending on the dendrimer concentration and the ion content. Scherrenberg et al.[26] and Ramzi et al.[27] have studied the molecular characterization of poly(propylene imine) dendrimer and the interdendrimer interference as a function of dendrimer concentration and solution acidity. In the present work, we perform the external contrast variation examination of SANS, which has never reported by previous investigators.

Experimental Section

Fifth- and sixth-generation PAMAM dendrimers with hydroxyl end groups (Chart 1) was synthesized by the reaction of 2-aminoethanol with 4.5- and 5.5-generation PAMAM dendrimer having methyl ester end groups.[16] Numbers of terminal hydroxyl groups of the fifth- and sixth-generation PAMAM dendrimer were determined to be 120 and 222, respectively, by ^1H NMR measurement. Calculated molecular weights of the fifth- and sixth-generation PAMAM in consideration of the inevitable defects of branches are 27 700 and 53 600, respectively. The degree of molecular weight distribution (M_w/M_n) estimated by size exclusion chromatography was 1.01 (eluent: 50 mM K_2HPO_4 aq, globular protein standard, 27 °C, Superdex 200HR 10/30 column). The hydrodynamic radii (R_H) determined by dynamic light scattering were 39 and 41 Å, respectively, for the fifth and sixth generation.[28] Ultrapure (Milli-Q) water was used as solvent, except solvents for SANS measurements. D_2O for SANS measurements was purchased from Wako Pure Chemical Industries, Ltd.

Chart 1. Chemical Structure of Fifth-Generation PAMAM Dendrimer with Hydroxyl End Group

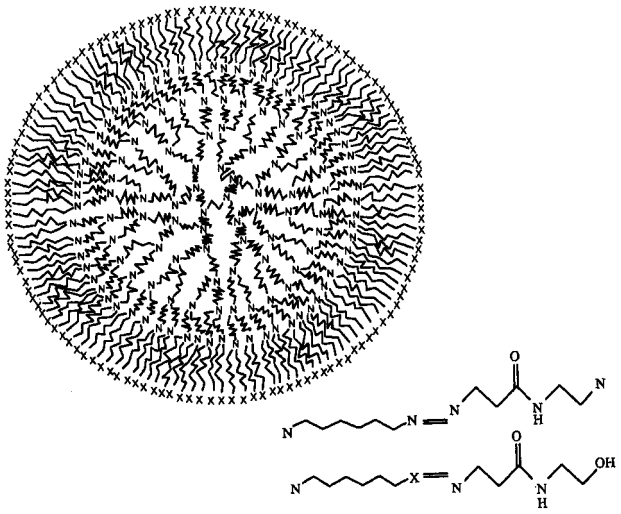

The microscopic observation was performed at room temperature (∼25 °C) by a Digital Instruments NanoScope III AFM. Images were recorded by the tapping mode. The fifth-generation dendrimers were adsorbed on freshly cleaved mica for 10 min from an aqueous solution of 10^{-4} wt % and dried in vacuo overnight.

The SANS measurements were performed using the cold neutron small-angle scattering instrument WINK in KEK. The instrument was operated at a neutron radiation of 1−16 Å wavelength at room temperature (∼25 °C). The SANS intensities $I(Q)$ were obtained as a function of scattering vector amplitude Q ($=(4\pi/\lambda)\sin(\theta/2)$), where λ is the neutron radiation wavelength and θ is the scattering angle. The intensity calibration and background subtraction were carried out according to the previously reported methods.[29,30] The rectangular quartz cell of 22 × 40 × 2 mm was used. Solvents for SANS measurements were D_2O and D_2O-H_2O mixtures. The mixing ratio is denoted by % H_2O ($=H_2O/(D_2O + H_2O)$ v/v %).

The surface force was measured at room temperature (∼25 °C) on an Anutech MASIF. Two glass beads were held on a piezo tube and Teflon-sheathed bimorph, respectively. The movement of the upper glass surface was measured by linear variable displacement transducers (LVDT) attached to piezo tube, and the movement of lower glass surface was measured as a displacement of bimorph and sent to a charge amplifier. The force run was carried out on "inward" and "outward" processes. From the variations of z piezo LVDT voltage and bimorph voltage on both processes, the deflection of bimorph was calculated as a function of time, and the force F divided by average radius of curvature of glass beads R was calculated as a function of separation between two glass surfaces. The deflection constant determined by interferometry was 0.526 μm/V. The spring constant of bimorph (∼200 N/m) was determined by the weight method, and the average radius of curvature of glass beads (∼1.2 mm) was measured by micrometer.

Results

Microscopic Observation. An AFM image in Figure 1 was obtained with a specimen prepared by adsorbing fifth-generation dendrimers on mica from 10^{-4} wt % aqueous solution. The AFM image displayed texture which

(22) Thornton, A.; Bloor, D.; Cross, G. H.; Szablewski, M. *Macromolecules* **1997**, *30*, 7600.
(23) Aoi, K.; Motoda, A.; Okada, M.; Imae, T. *Macromol. Rapid Commun.* **1997**, *18*, 945.
(24) Aoi, K.; Itoh, K.; Okada, M. *Macromolecules* **1997**, *30*, 8072.
(25) Tokuhisa H.; Crooks, R. M. *Langmuir* **1997**, *13*, 5608.
(26) Scherrenberg, R.; Coussens, B.; van Vliet, P.; Edouard, G.; Brackman, J.; de Brabander, E. *Macromolecules* **1998**, *31*, 456.
(27) Ramzi, A.; Scherrenberg, R.; Brackman, J.; Joosten, J.; Mortensen, K. *Macromolecules* **1998**, *31*, 1621.
(28) Imae, T.; Funayama, K.; Aoi, K.; Tsutsumiuchi, K.; Okada, M. *Proc. Yamada Conf.*, in press.
(29) Chen, S. H. *Annu. Rev. Phys. Chem.* **1986**, *37*, 351.
(30) Chen, S. H.; Lin, T. L. *Methods Exp. Phys.* **1987**, *23*, 489.

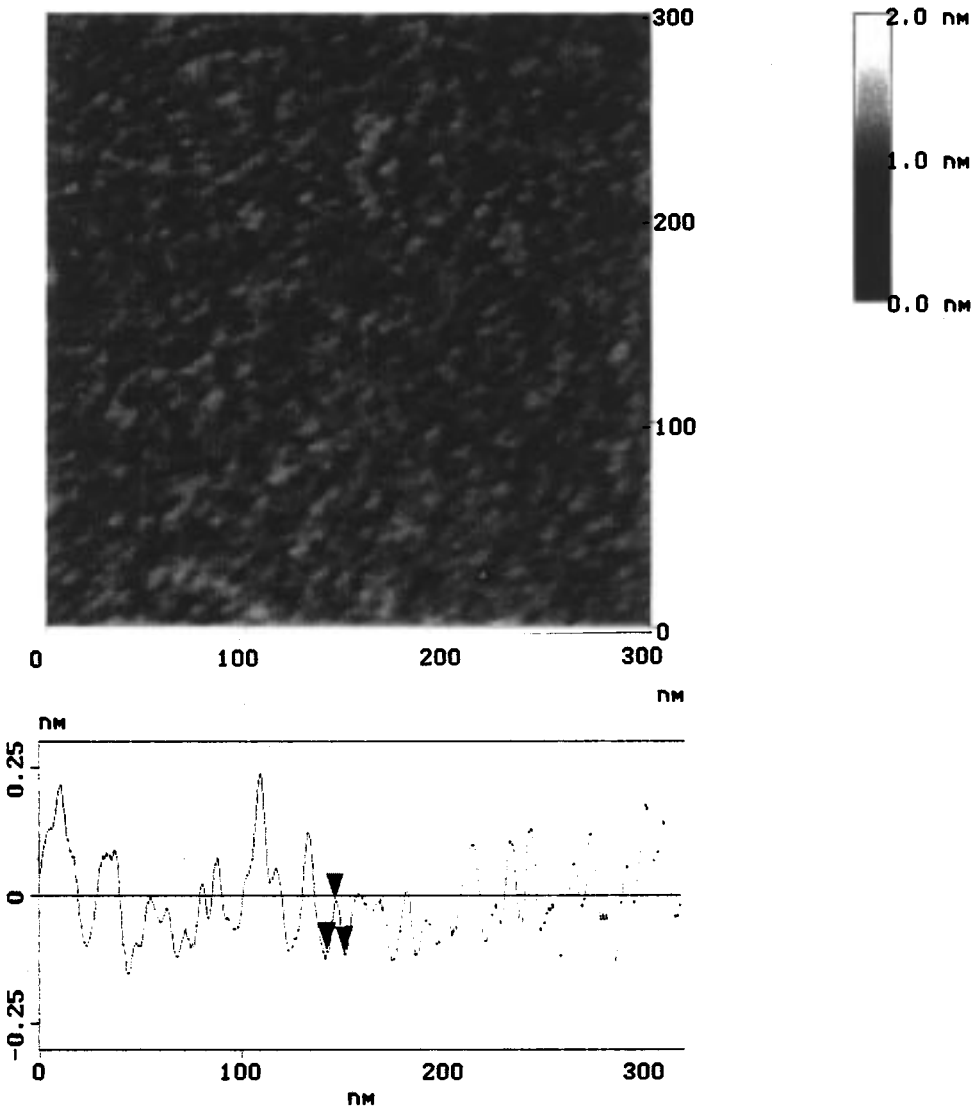

Figure 1. An AFM image of fifth-generation PAMAM dendrimers adsorbed on mica for 10 min from a 10^{-4} wt % aqueous solution. The lower figure represents the section analysis.

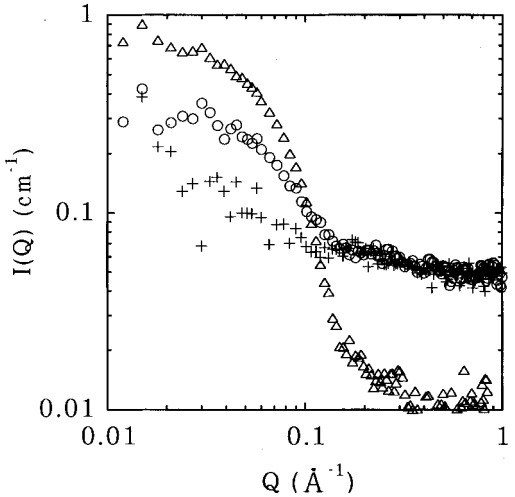

Figure 2. A double logarithmic plot of SANS intensity vs scattering vector magnitude for fifth-generation PAMAM dendrimer solutions of different mixing ratios in D_2O-H_2O mixture. % H_2O: △, 0; ○, 25; +, 50. Dendrimer concentration is 1.0 wt %.

is assigned to dendrimers. The dendrimers were adsorbed on a mica substrate with the surface height difference of only about 2 Å. This value is far smaller in comparison with the dendrimer height, indicating the formation of a rather flat surface.

Small-Angle Neutron Scattering. Figure 2 shows double logarithmic plots of SANS intensity $I(Q)$ vs scattering vector magnitude Q for the fifth-generation dendrimer solutions of 0, 25, and 50% H_2O. Although the scattering vector dependence of SANS intensities was remarkable at 0% H_2O, it became dull with increasing H_2O content.

The SANS intensity as a function of scattering vector magnitude is written as

$$I(Q) = n_p P(Q) \quad (1)$$

for dilute solutions,[29−35] as in the case of the present work,

(31) Guinier, A.; Fournet G. *Small-angle Scattering of X-ray*; Wiley: New York, 1955.
(32) Glatter, O.; Kratky, O. *Small-Angle X-ray Scattering*; Academic Press: London, 1982.
(33) Feigin, L. A.; Svergun, D. I. *Structure Analysis by Small-Angle X-ray and Neutron Scattering*; Taylor, G. W., Ed. Plenum: New York, 1987.
(34) Lindner, P.; Zemb, Th. *Neutron, X-ray and Light Scattering: Introduction to an Investigative Tool for Colloidal and Polymeric Systems*, North-Holland: Amsterdam, 1991.
(35) Imae, T. *Colloids Surf.* **1996**, *109*, 291.

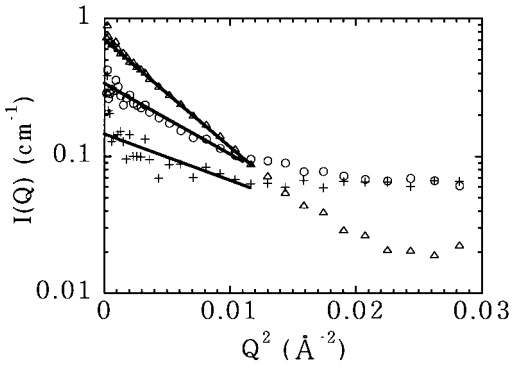

Figure 3. Guinier plots for fifth-generation PAMAM dendrimer solutions of different mixing ratios in D_2O-H_2O mixture. % H_2O: △, 0; ○, 25; +, 50. Dendrimer concentration is 1.0 wt %. Solid lines represent the fitting to a Guinier equation.

where the interparticle scattering factor approaches unity. n_p is the number density of colloidal particles, and $P(Q)$ is the intraparticle structure factor which depends on the particle geometry. For homogeneous spherical particles of radius of gyration R_G, if QR_G values are small, the intraparticle structure factor is described by a Guinier equation of

$$P(Q) = V^2(\rho - \rho_s)^2 \exp(-R_G{}^2Q^2/3) \quad (2)$$

where V is the total volume of a particle, and ρ and ρ_s are the mean coherent neutron scattering length densities of the particle and the solvent, respectively. Then

$$\ln I(Q) = \ln I(0) - R_G{}^2Q^2/3 \quad (3)$$

$$I(0) = n_pV^2(\rho - \rho_s)^2 = n_p(b_m - v_m\rho_s)^2 \quad (4)$$

where b_m is the sum of scattering lengths of all the nuclei constituting the particle and v_m is the dry or solvent-excluded volume of the particle. When the external contrast variation method is applied by varying the mean coherent neutron scattering length density of the solvent

$$\rho_s = (1 - \alpha)\rho_{H_2O} + \alpha\rho_{D_2O} \quad (5)$$

where $1 - \alpha$ is the fractional number of H_2O molecules in the solvent, that is, % H_2O.[29,30] ρ_{H_2O} and ρ_{D_2O} are the mean coherent neutron scattering length densities of H_2O and D_2O, respectively. The introduction of eq 5 into eq 4 results in

$$I(0)^{1/2} = n_p{}^{1/2}(b_m - v_m\rho_{D_2O}) - n_p{}^{1/2}v_m(\rho_{H_2O} - \rho_{D_2O})(1 - \alpha) \quad (6)$$

One can notice from eqs 3−6 that the Guinier plot, that is, the plot of logarithmic $I(Q)$ against Q^2 is linear. Moreover, $I(0)^{1/2}$ values change linearly with the variation of ρ_s or $1 - \alpha$ values.

As seen in the Guinier plot of Figure 3, the linear relation existed between the logarithmic $I(Q)$ and Q^2 at the small scattering vector region below 0.01 Å^{-2}. The apparent R_G values, which were evaluated from eq 3 and plotted in Figure 4 as a function of % H_2O, decreased remarkably with increasing % H_2O. The SANS intensities $I(0)$ at zero scattering vector were obtained from the extrapolation of the Guinier plot and plotted in Figure 5. The $I(0)^{1/2}$ values linearly decreased, as expected, when % H_2O is increased.

Surface Force Measurement. Surface forces were measured between glass beads adsorbed dendrimers from

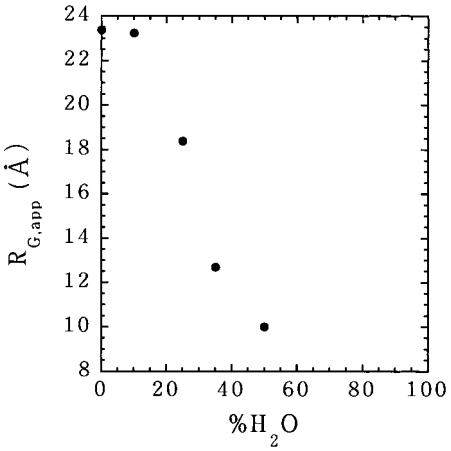

Figure 4. Apparent R_G values as a function of % H_2O for fifth-generation PAMAM dendrimer solutions. Dendrimer concentration is 1.0 wt %.

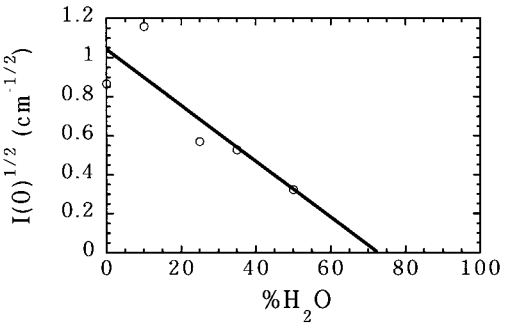

Figure 5. Square root of SANS intensities $I(0)$ at zero scattering angle as a function of % H_2O for fifth-generation PAMAM dendrimer solutions. Dendrimer concentration is 1.0 wt %.

10^{-7} and 10^{-3} wt % aqueous solutions of the fifth-generation dendrimer and a 10^{-3} wt % solution of the sixth-generation dendrimer. Figure 6 shows the adsorption time dependence of surface force−separation curves for a 10^{-3} wt % aqueous solution of the fifth-generation dendrimer. The force−separation curves on the inward and outward processes at 1 h adsorption were both the same as those between glass surfaces without dendrimers in water, which is included in Figure 6. The repulsive force at the inward process decreased with increasing adsorption time up to 4 h but increased again at 12 h adsorption. On the outward process, the jump-out occurred at 2 h adsorption. Although the adhesion force to be the jump-out force increased at 4 h adsorption, it disappeared at 12 h. It should be noted that the force−separation curve on the outward process at 12 h adsorption was almost the same as that on the inward process.

Similar adsorption time dependence of the force curves was also observed for a 10^{-7} wt % solution of the fifth-generation dendrimer[28] and a 10^{-3} wt % solution of the sixth-generation dendrimer. The latter results are given in Figure 7. The variation of the force curves occurred at longer adsorption time for lower dendrimer concentration but at shorter adsorption time for higher generation. The adhesion forces for the fifth generation were independent of concentration to be 1.2−2.2 mN/m, while it was weaker than that (2.4−5.0 mN/m) for the sixth generation.

Discussion

The sizes of fifth- and sixth-generation PAMAM dendrimers with hydroxyl end groups have been determined by dynamic light scattering.[28] Although the obtained values are within the possible size range which was

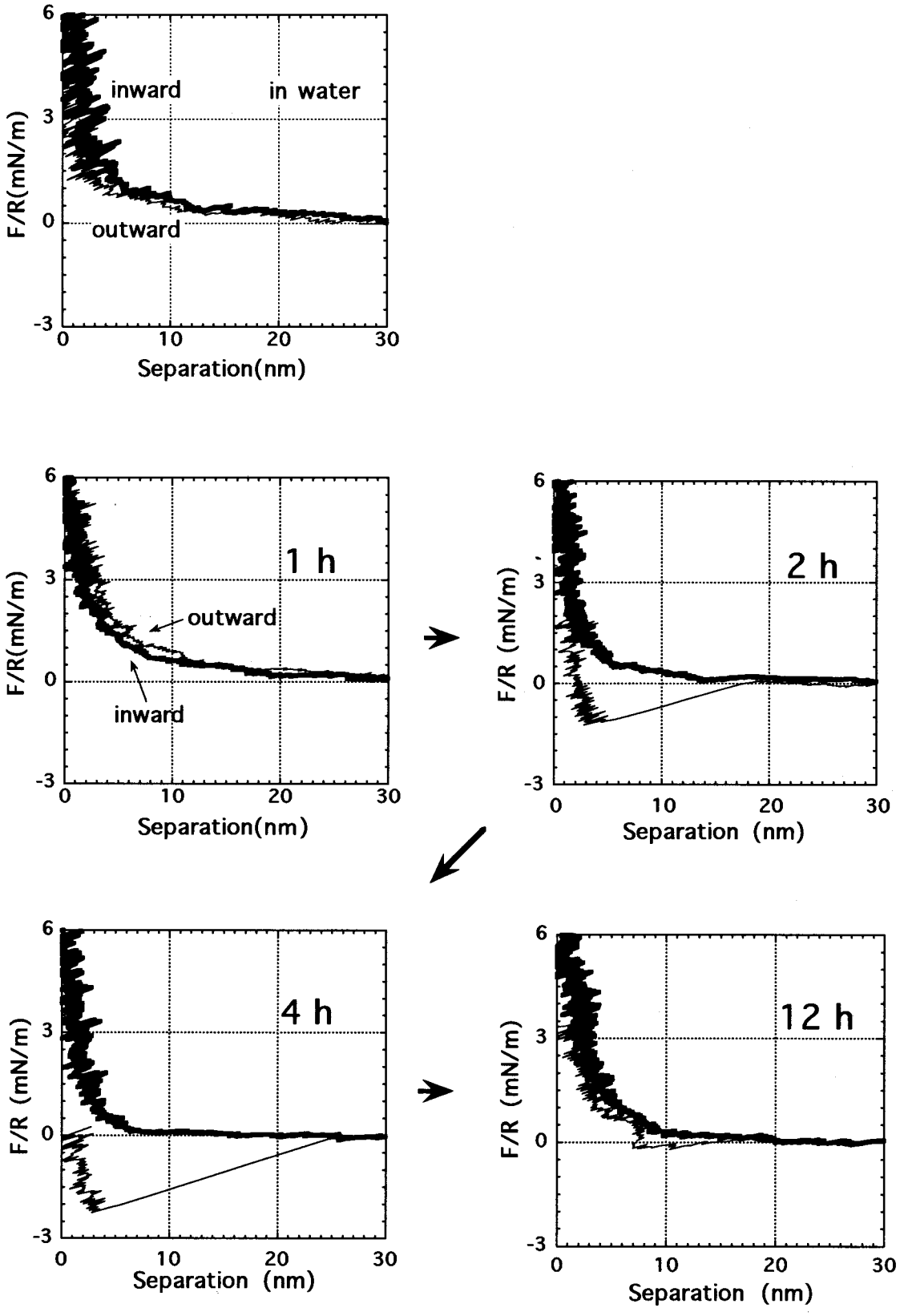

Figure 6. Force vs separation curves in water without dendrimer and for 1, 2, 4, and 12 h adsorption from a fifth-generation PAMAM dendrimer solution. Dendrimer concentration is 10^{-3} wt %.

calculated by the Corey−Pauling−Koltum (CPK) model,[23] those are rather closer to the more extended chain model. The texture of dendrimer was observed by AFM (Figure 1). The adsorption surface of dendrimers on mica substrate is flatter than the surface where a tiny amount of aqueous dendrimer solution was dropped on mica and dried.[28] Such flattening of adsorption surface may occur from the variation of dendrimer shape on substrate, as suggested before.[7,19,36] Dendrimers adsorbed on mica in the present

(36) Sheiko, S. S.; Gauthier, M.; Möller, M. *Macromolecules* **1997**, *30*, 2343.

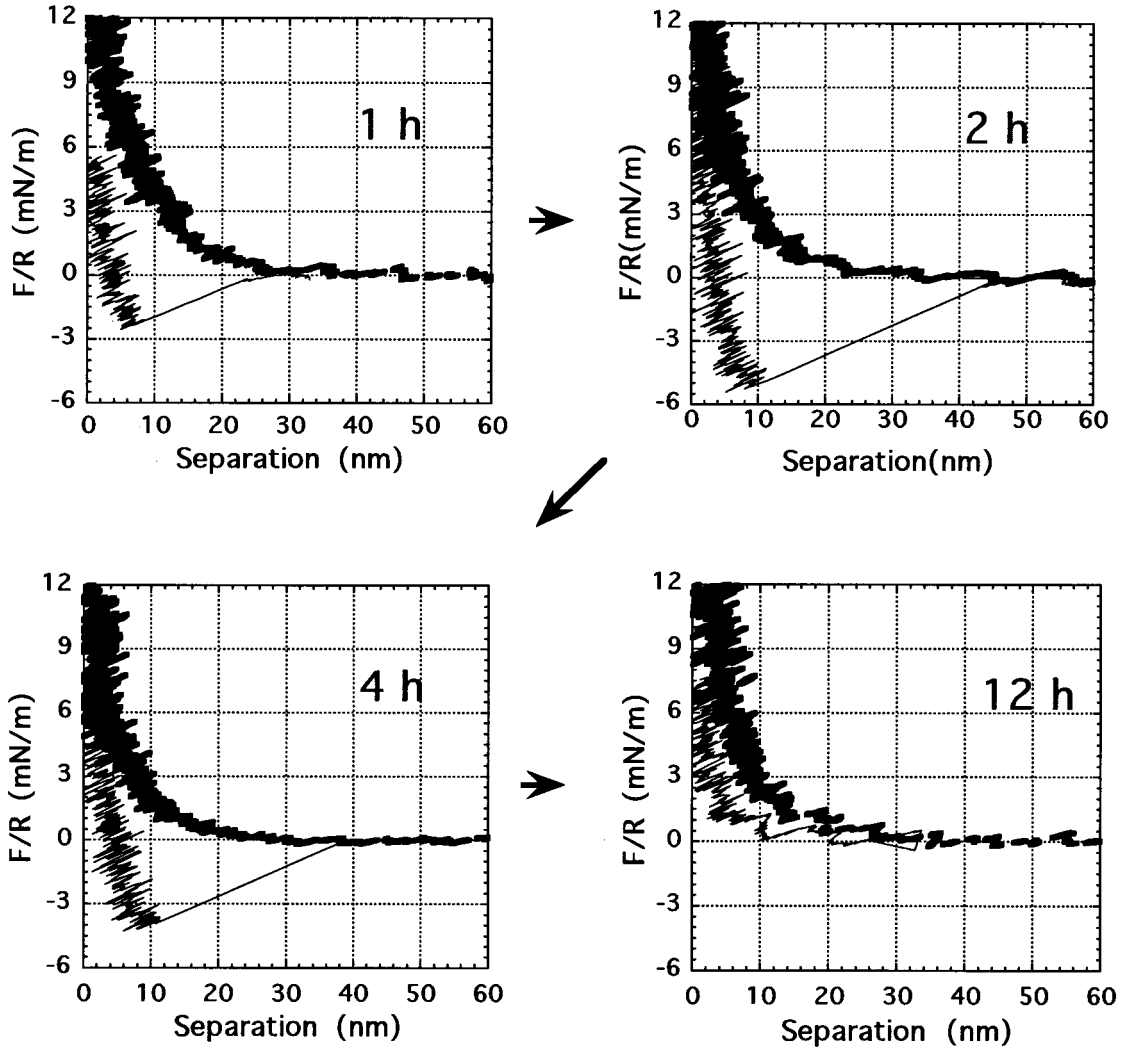

Figure 7. Force vs separation curves for 1, 2, 4, and 12 h adsorption from a sixth-generation PAMAM dendrimer solution. Dendrimer concentration is 10^{-3} wt %.

work are not arranged with regularity, in contrast with the report by Sheiko et al.[36] They have visualized the molecular organization of arborescent graft polystyrenes in monomoleculer films cast on mica. Coen et al.[7] have reported the surface topographies of thin cast films of mesogen-substituted carbosilane dendrimers on mica but have never referred to the dendrimer image. The electron microscopic and AFM observations have also been carried out for the aggregation morphology of polystyrene−dendrimer amphiphilic block copolymers[4,5] and monodendrons.[9,10]

The analysis of the Guinier plot on the basis of eqs 3−5 indicates the linearity of the plots of logarithmic $I(Q)$ against Q^2 at the small scattering vector region and of $I(0)^{1/2}$ against % H_2O, as estimated. From the latter plot (Figure 5), one can obtain the matching point at 72.6% H_2O, where the mean coherent neutron scattering length density of the dendrimer is equivalent to that of the solvent. Moreover, $v_m = 38\ 500$ Å^3 and dendrimer molecular weight $M = 0.01/(n_p/N_A) = 21\ 300$ are evaluated from a linear relation in Figure 5 and eq 6, where $b_m = 515 \times 10^{-12}$ cm, $\rho_{D_2O} = 6.36 \times 10^{-14}$ cm Å^{-3}, and $\rho_{H_2O} = -0.56 \times 10^{-14}$ cm Å^{-3}. N_A is Avogadro's number. The evaluated molecular weight is close to the calculated one described in the Experimental Section.

On the other hand, the apparent R_G values obtained from Figure 3 decrease remarkably with increasing % H_2O, as seen in Figure 4. This is different from a result which has been obtained on the external contrast variation examination for surfactant micelles.[29,37] On the SANS measurement of AOT in decane, the radii of gyration calculated from the slope of the Guinier plot are not varied within the weight ratio of deuterated to protonated decane of 0.41−0.98. In the present case, the ramarkable variation of radius of gyration depending on the % H_2O suggests the penetration of water into dendrimers. The radius of gyration calculated from a relation of $R_G^2 = 3R_H^2/5$ for rigid sphere and a value of $R_H = 39$ Å is 30 Å for the fifth-generation dendrimer. It is obvious from the comparison with the apparent radius of gyration of 23.4 Å observed from SANS in D_2O (0% H_2O) that the mean coherent neutron scattering length density in dendrimer domain is added by that of solvent penetrated into dendrimer.

Dendrimers are synthesized by adding segment units stepwise to a starting core in order to form the generations. Therefore, the segment density in dendrimer may change from core to exterior. For the purpose of elucidating the segment distribution, the analysis which has been done by Stuhrmann et al.[38−40] is applied for SANS data in the present work. Suppose that the mean coherent neutron

(37) Kotlarchyk, M.; Huang, J. S.; Chen, S. H. *J. Phys. Chem.* **1985**, *89*, 4382.
(38) Stuhrmann, H. B.; Fuess, H. *Acta Crystallogr.* **1976**, *A32*, 67.
(39) Jacrot, B. *Rep. Prog. Phys.* **1976**, *39*, 911.
(40) Stuhrmann, H. B.; Miller, A. J. *Appl. Crystallogr.* **1978**, *11*, 325.

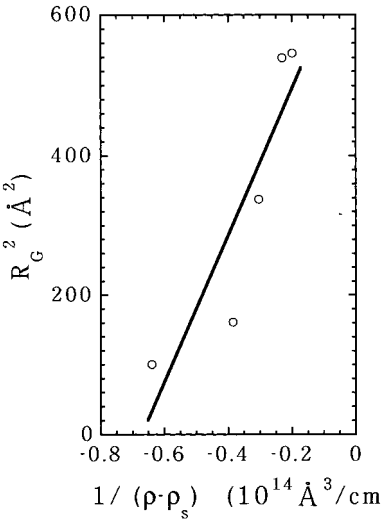

Figure 8. Variation of the square of the radius of gyration plotted against the reciprocal of the contrast $\rho - \rho_s$ for fifth-generation PAMAM dendrimer solutions of different mixing ratios in a D_2O-H_2O mixture. Dendrimer concentration is 1.0 wt %.

scattering length density of the particle is an average value, over the volume V, of the local scattering length density $\rho(r)$ at the radial distance r from a particle center, that is

$$\rho = (1/V)\int_v \rho(r)\, d^3r \tag{7}$$

$\rho(r)$ is split into two parts:

$$\rho(r) = \rho + \Delta\rho(r) \tag{8}$$

where $\Delta\rho(r)$ is a fluctuation of the density around the mean value and defined by

$$\int_v \Delta\rho(r)\, d^3r = 0 \tag{9}$$

Now, a radius of gyration R_G is given by the expression

$$R_G^2 = \{1/(\rho - \rho_s)V\}\int_v \{\rho(r) - \rho_s\}\, r^2\, d^3\, r \tag{10}$$

By using eq 8

$$R_G^2 = R_{Gv}^2 + \{1/(\rho - \rho_s)V\}\int_v \Delta\rho(r)\, r^2\, d^3\, r \tag{11}$$

and

$$R_{Gv}^2 = (1/V)\int_v r^2\, d^3\, r \tag{12}$$

Figure 4 is replotted in Figure 8 as a variation of R_G^2 against the reciprocal of $(\rho - \rho_s)$. Then a positive slope is obtained. This supports that there is the segment density distribution in the dendrimer, according to eq 11, where $\int_v \Delta\rho(r)\, r^2\, d^3\, r$ is positive.

Suppose that the spherical fifth-generation dendrimer consists of concentric five layers, as depicted in Figure 9, since generations of the dendrimer can be regarded as the distinguished layers with different segment density, although each layer has a mean density. Then the intradendrimer structure factor is contributed by the terms from an internal core of radius R_1 and the

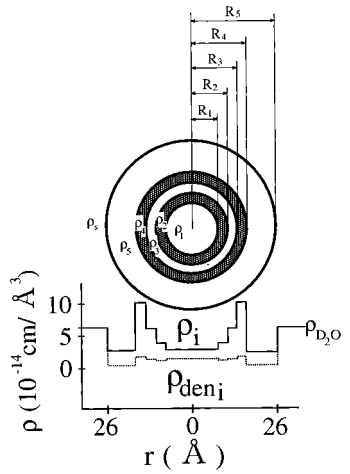

Figure 9. Geometric definition and density profile of spherical particle with concentric structure. Five layers geometry (upper) and coherent neutron scattering density profile (lower) of fifth-generation PAMAM in D_2O as a function of radial distance from the concentric center.

Table 1. Parameters Used and Obtained in SANS Calculation for a 1.0 wt % Solution of Fifth-Generation Dendrimer in D_2O

	$i = 1$	$i = 2$	$i = 3$	$i = 4$	$i = 5$
R_i, Å	8	11	14	17	26
ρ_{deni}, 10^{-14} cm Å^{-3}	1.4	1.1	1.3	1.7	0.4
ρ_i, 10^{-14} cm Å^{-3}	2.8	3.9	6.2	10	2.6
A_i	15	50	150	400	620
$A_{i/segment}$	2	3	5	6	5

surrounding shells with thickness of $R_i - R_{i-1}$ as follows;

$$P(Q) = [\sum_{i=1}^{4}(4\pi R_i^3/3)\,(\rho_i - \rho_{i+1})\{3J_1(QR_i)/QR_i\} + (4\pi R_5^3/3)\,(\rho_5 - \rho_s)\{3J_1(QR_5)/QR_5\}]^2 \tag{13}$$

where ρ_i is the mean coherent neutron scattering length density in the ith layer of a dendrimer, and $J_1(x) = (\sin x - x\cos x)/x$ is the first-order Bessel function. When the solvent penetrates into dendrimers, ρ_i must be contributed from the penetrating solvent besides dendrimer. Then

$$\rho_i = \rho_{deni} + A_i\rho_s \tag{14}$$

where ρ_{deni} is the mean coherent neutron scattering length density of dendrimer segment in the ith layer and A_i is the number density of the solvent in the ith layer.

When the parameters listed in Table 1 are used for calculation of SANS intensity by using eqs 1, 5, 13, and 14 for the five-layer model under the consideration of water penetration, the best fit curve for an aqueous D_2O solution of a fifth-generation dendrimer is obtained at the range up to $Q = \sim 0.4$ Å^{-1}, as shown in Figure 10. The neutron scattering length density profile is illustrated in Figure 9, and the penetrated water per segment residue $A_{i/segment}$ is listed in Table 1. The fitting curves, where the same parameters in Table 1 are applied to the solutions of higher H_2O content, is better at a lower scattering vector region but less at a higher scattering vector region. It can be noticed from Table 1 that the most exterior layer is thickest because of the extension of segment chains. However, the segment density proportional to the ρ_{deni} illustrated in Figure 9 is lower at the fifth layer in comparison with the other layers. It can be interpreted that, at the fifth layer, the segment density increase by the segment branching is overcome by the density decrease due to the segment

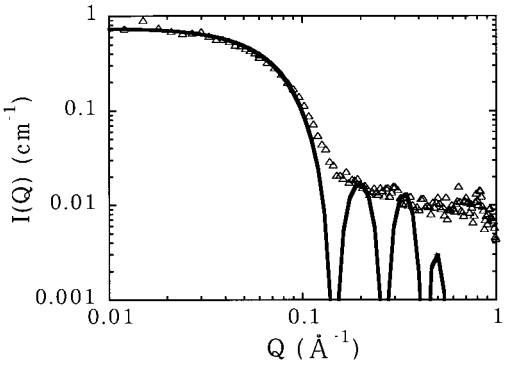

Figure 10. Double logarithmic SANS profile for a 1.0 wt % solution of fifth-generation PAMAM dendrimer in D_2O: △, observed; solid line, calculated on five-layer model with penetrated water.

chain extension. On the other hand, the water penetration A_i increases from interior to exterior. It may be noticed that water penetration per segment is six at most. Thus ρ_i, which is contributed by the segment density and the penetrated water content, is the highest at the fourth generation for the D_2O solution, as seen in Figure 9.

The fact of water penetration in dendrimer and, therefore, the existence of a solvent-filled void are remarkable in connection with the ability of dendrimer doping small molecules. The density distribution in dendrimer has been discussed by some investigators.[16,26,41−43] De Gennes and Hervet[41] have predicted from the theoretical treatment that a segment distribution function has the highest density on the periphery with relatively hollow cores. On the contrary, Lescanec and Muthukumar[42] infer the highest density at the center and a decaying profile to the edge of dendrimer. On a report of Meltzer et al.,[16] whole dendrimer density is lowest at fifth and sixth generations, while surface layer density increases with increasing generation and outstrips the whole dendrimer density above the eighth generation. Meltzer et al. suggest the folding back of terminal groups into the interior of the higher (ninth or tenth) generation dendrimers. The theoretical prediction of Boris and Rubinstein[43] is a monotonic decrease of dendrimer density from the center to the surface and a maximum profile of free end probability. Scherrenberg et al.[26] also report that the end groups are distributed throughout the dendrimer. It is confirmed that for the fifth-generation dendrimer in the present work, the segment density profile is owing to the compensation of the segment density increase by the segment branching and the density decrease due to the segment chain extension, although the solvent-filled void depends on the latter fact.

The surface force−separation curves between glass beads adsorbed dendrimers depend on adsorption time (see Figures 6 and 7). At the initial adsorption, the force−separation curve is equivalent to that between glass surfaces in water without dendrimers, because dendrimer molecules do not adsorb or adsorb poorly on glass surfaces. At the medium adsorption time, the repulsive force on the inward process is weaker than that between glass surfaces without adsorbed dendrimers and the adhesion force occurs on the outward process. Dendrimers adsorb dispersively on the glass surfaces. Since the real contact surfaces are no longer at the glass surfaces, the electrostatic repulsion force between glass surfaces diminishes apparently. Moreover, the monolayer of dendrimers formed between glass surfaces in contact induces the adhesive attraction force between dendrimer and glass. At the long adsorption time, since both glass surfaces are covered by adsorbed dendrimers, the repulsive force acts between dendrimer layers.

The interaction force acting between two spheres at constant temperature T and pressure P is related to the interaction potential V_{pp} between two flat plates by Derjaguin's approximation, that is, $F/R = \pi V_{pp}$. When two polymer layers adsorbed on plates approach each other, the interaction potential is described by the sum of the van der Waals attraction potential and the steric repulsion potential, if the electrostatic repulsion potential is negligible as the case of the adsorption of nonionic dendrimers in the present work. When the plates with adsorbed polymer layers are thicker than the interlayer distance H_{pp}, the van der Waals potential V_A is written by

$$V_A = -A/(12\pi H_{pp}^2) \quad (15)$$

where A is the Hamaker attraction constant. A value of 10^{-20} J can be chosen as the Hamaker attraction constant for dendrimers.[44]

The mixing or osmotic effect V_M and the volume restriction effect V_{VR} in the steric repulsion potential on the adsorption layer of linear polymers have been derived by Meier[45] and Hesselink[46] as follows:

$$V_M = 2(2\pi/9)^{3/2}\nu^2 RT(\alpha_e^2 - 1)\langle h^2\rangle 3\pi^{1/2}(6H_{pp}^2/\langle h^2\rangle - 1)\exp(-3H_{pp}^2/\langle h^2\rangle) \quad (16)$$

and

$$V_{VR} = 2\nu kT2(1 - 12H_{pp}^2/\langle h^2\rangle)\exp(-6H_{pp}^2/\langle h^2\rangle) \quad (17)$$

where ν is the number of loops and tails per unit area or the amount of polymer adsorbed, α_e is the expansion of a chain, $\langle h^2\rangle^{1/2}$ is the root-mean-square end-to-end distance of the chain, R is the gas constant, and k is the Boltzmann constant. The prediction of the dispersion stabilization by adsorbed polymer has been carried out, on the basis of eqs 15−17, by Hesselink et al.[44] When the adsorption layer of linear polymers is replaced by the layer of dendrimers, parameters can be determined as follows: $\alpha_e = 1.2$ and $kT = 4.12 \times 10^{-21}$ J. Moreover, $\nu = 6.70 \times 10^{-3}$ Å^{-2} and $\langle h^2\rangle = 1520$ Å^2 for the fifth-generation dendrimer and $\nu = 12.1 \times 10^{-3}$ Å^{-2} and $\langle h^2\rangle = 1680$ Å^2 for the sixth-generation dendrimer.

While the volume restriction repulsion is due to the decrease of configurational entropy of an adsorbed polymer on the approach of a second polymer, the osmotic repulsion results from the mixing of the adsorbed polymer clouds. The calculated osmotic repulsion is more effective and predominant on the interaction between dendrimer layers than the volume restriction repulsion, whereas the contribution of van der Waals attraction is negligible except for the nearest approach. The calculated total interaction potentials for the fifth- and sixth-generation dendrimer are plotted as a function of the distance in Figure 11. The evaluated total potential for the sixth-

(41) de Gennes, P.-G.; Hervet, H. *J. Phys. (Paris)* **1983**, *44*, L351.
(42) Lescanec, R. L.; Muthukumar, M. *Macromolecules* **1990**, *23*, 2280.
(43) Boris, D.; Rubinstein, M. *Macromolecules* **1996**, *29*, 7251.
(44) Hesselink, F. Th.; Vrij, A.; Overbeek, J. Th. G. *J. Phys. Chem.* **1971**, *75*, 2094.
(45) Meier, D. J. *J. Phys. Chem.* **1967**, *71*, 1861.
(46) Hesselink, F. Th. *J. Phys. Chem.* **1969**, *73*, 3488; **1971**, *75*, 65.

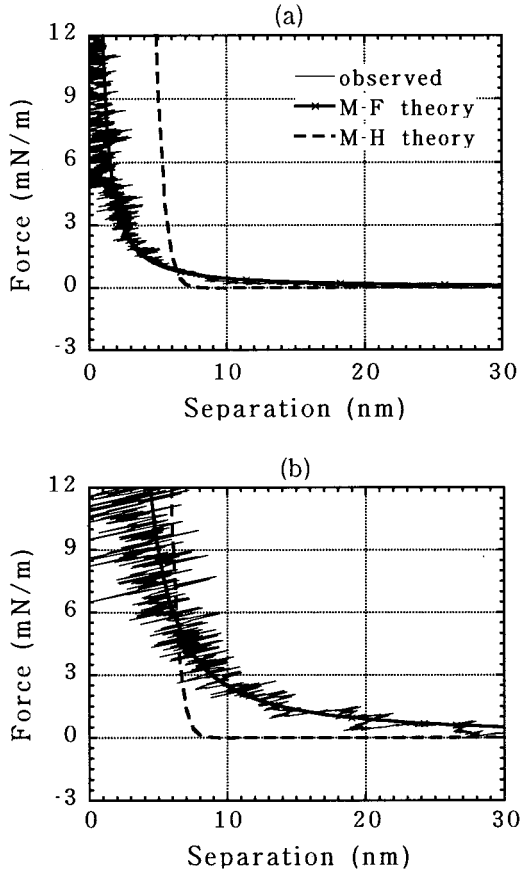

Figure 11. Observed and calculated force vs separation curves for 12 h of adsorption from a PAMAM dendrimer solution. Dendrimer concentration is 10^{-3} wt %. (a) fifth-generation; (b) sixth-generation. —, observed; —×— calculated total interaction potential between plates coated by adsorbed dendrimers on the basis of the theory of Meier[45] and Hesselink;[46] - - -, calculated osmotic pressure term of interaction potential between plates coated by adsorbed dendrimers on the basis of the theory of Marques et al.[48] and Fredrickson et al.[49]

generation dendrimer is slightly larger than that for the fifth-generation dendrimer, as assumed. However, when the calculated interaction potentials for the fifth- and sixth-generation dendrimer are compared with the observed force−separation curves at 12 h adsorption where glass surfaces are much covered by adsorbed dendrimers, one can recognize that the calculated values are qualitatively reproducible with the observed one but the quantitative consistency is not necessarily good. The reason may be the difference of adsorption layer between linear polymers and dendrimers.

Pelletier et al.[47] have investigated the adsorption kinetics of a diblock copolymer by means of a surface force apparatus. They demonstrate that the forces measured for ultrathin layers of polystyrene/poly(2-vinylpyridine) diblock copolymer in toluene are dominated by the osmotic

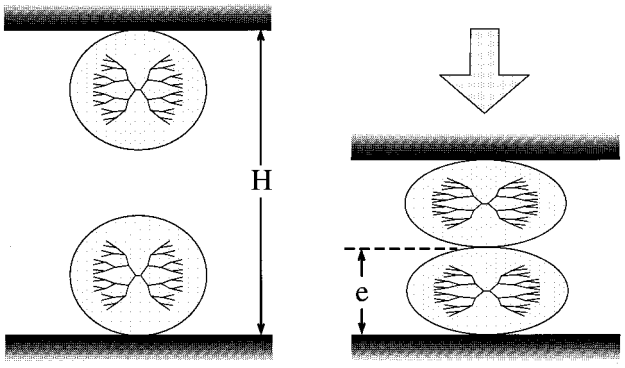

Figure 12. Schematic illustration of glass surfaces with adsorbed dendrimers before contact (left) and after contact (right).

pressure term which is written by the relation of[47−49]

$$F/R = (A\Gamma)^{9/4}(H - 2e)^{-5/4} \qquad (18)$$

where Γ is the number of adsorbed molecules per surface area, A is a constant, H is the closest distance between glass surfaces, and e is a thickness of "molten" or "squeezed" polymer. It seems that the model for the theory is applicable for fifth- and sixth-generation PAMAM with hydroxyl end groups in the present work. Then e correponds a thickness of "pancake" dendrimer sandwiched between two surfaces in contact (see Figure 12). As seen in Figure 11, the calculation based on eq 18 fits well to the observation at 12 h adsorption, when the optimum numerical values of $A\Gamma = (7.6 \text{ and } 32) \times 10^{-6}$ N$^{4/9}$ m$^{1/9}$ and $e = 1.5$ and 11 Å are adopted for fifth- and sixth-generation, respectively. Then it is confirmed that the molecular adsorption and the pancake thickness are more predominant for sixth-generation than for fifth-generation, as expected. However, since the adsorption thickness is too thin in comparison with calculated diameters of spherical dendrimers 22−48 Å, it is assumed that the dendrimers adsorb less than monolayer.

It can be confirmed from the present work that the interaction potential between layers of PAMAM dendrimer with hydroxyl end groups is mainly steric repulsion. This indicates that the dendrimer with repulsive intermolecular interaction can be utilized as a surface-improvement agent promoting the dispersion stability of fine particles in medium. Although linear polymers are used for such a purpose, the behavior of particles coated by linear polymers is rather complicated, owing to the roughness of loop region, the bridging effect, and the depletion effect. The dendrimer coating will reduce such complications.

Acknowledgment. This work was supported by New Energy and Industrial Technology Development Organization (NEDO) for the project on Technology for Novel High-Functional Materials in Industrial Science and Technology Frontier Program, AIST.

LA9811968

(47) Pelletier, E.; Stamouli, A.; Belder, G. F.; Hadziioannou, G. *Langmuir* **1997**, *13*, 1884.

(48) Marques, C.; Joanny, J. F.; Leibler, L. *Macromolecules* **1988**, *21*, 1051.

(49) Fredrickson, G. H.; Pincus, P. *Langmuir* **1991**, *7*, 789.